Journal Pre-proofs

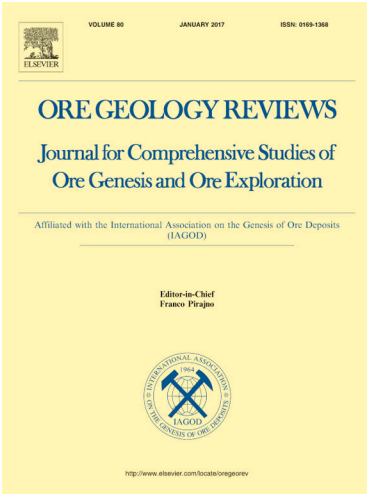

Geochronology and geochemistry of the PiaOac granites: Implication for Late Cretaceous magmatism and metallogeny in NE Vietnam

DinhLuyen Nguyen, Rucheng Wang, Jinhai Yu, Xiao-Lei Wang, QuangLuat Nguyen, TrungHieu Pham, VanNhuan Do

PII: S0169-1368(22)00035-X
DOI: https://doi.org/10.1016/j.oregeorev.2022.104727
Reference: OREGEO 104727

To appear in: *Ore Geology Reviews*

Received Date: 23 February 2021
Revised Date: 16 January 2022
Accepted Date: 24 January 2022

Please cite this article as: D. Nguyen, R. Wang, J. Yu, X-L. Wang, Q. Nguyen, T. Pham, V. Do, Geochronology and geochemistry of the PiaOac granites: Implication for Late Cretaceous magmatism and metallogeny in NE Vietnam, *Ore Geology Reviews* (2022), doi: https://doi.org/10.1016/j.oregeorev.2022.104727

Geochronology and geochemistry of the PiaOac granites: Implication for Late Cretaceous magmatism and metallogeny in NE Vietnam

DinhLuyen Nguyen[a,b], Rucheng Wang[a, *], Jinhai Yu[a, *], Xiao-Lei Wang[a], QuangLuat Nguyen[b], TrungHieu Pham[c]，VanNhuan Do[b].

[a]*State Key Laboratory for Mineral Deposits Research, School of Earth Sciences and Engineering, NanjingUniversity, Nanjing 210046, China*

[b]*HanoiUniversity of Mining and Geology, Hanoi, Vietnam*

[c]*Faculty of Geology, VNU-HCM University of Science, Vietnam*

luyenhumg@gmail.com

rcwang@nju.edu.cn

jhyu@nju.edu.cn

wxl@nju.edu.cn

luathumg@gmail.com

pthieu@hcmus.edu.vn

dovannhuan_humg@yahoo.com

*****Corresponding authors: Rucheng Wang and Jinhai Yu

Abstract

Sn-W deposits have recently been found in NE Vietnam, which has been considered as southwestern extension of the South China Block. The timing and relationships between the Sn-W mineralization and associated granitic magmatism in this area have not been well understood. This study presents new zircon and cassiterite U-Pb geochronology, whole-rock geochemistry, and zircon Hf-isotope data for the PiaOac granites, greisens, and cassiterite veins in NE Vietnam. The PiaOac granites are characterized by high Na_2O+K_2O, and K_2O/Na_2O, and low $Fe_2O_3^T$ and Mg#. The presence of primary muscovite, and high A/CNK (1.23-1.26), Rb/Sr (20-25), and P_2O_5 (0.33-0.35%) suggest that they are strongly peraluminous S-type granites. Low K/Rb, Zr/Hf, Nb/Ta, and Eu/Eu* indicate that the granitic magma experienced strong fractional crystallization. The PiaOac granites have homogeneous zircon Hf-isotope compositions with average $\varepsilon_{Hf}(t)$ values of -9.6 to -8.7 and two-stage Hf model ages of 1.76-1.71 Ga. They probably were sourced from Neoproterozoic metasedimentary rocks with late Paleoproterozoic model ages in NE Vietnam. Low CaO/Na_2O (<0.3) and high Rb/Sr and Rb/Ba ratios further suggest a clay-rich pelitic source. Zircons from greisen have significantly unradiogenic Hf-isotope compositions (ε_{Hf} (t) = -12.2) and large variations, implying strong interaction with wall rocks in late fluid-rich stage during magmatic evolution. Extended magmatic differentiation was followed by interaction with wall rocks, which has altered the redox environment, facilitating the Sn-W mineralization.

Zircon U-Pb dating results reveal that the PiaOac granites formed in the Late Cretaceous (89-88 Ma), coincident with the ~89 Ma mineralization constrained by cassiterite U-Pb dating, suggesting that the Sn-W mineralization is closely related to the granitic magmatism and greisenization. Late Cretaceous magmatism and mineralization in NE Vietnam are similar to those in SW South China in terms of formation age, rock association, deposit type, source composition, and tectonic setting, all together constituting an E-W trending Late Cretaceous metallogenic belt. The Late Cretaceous

granites and associated deposits in the belt were probably formed in an intracontinental orogenic setting in response to the combined action of the subduction of Pacific and Neo-Tethys Plates.

Key words: Late Cretaceous PiaOac granite; Zircon and cassiterite U-Pb dating; NE Vietnamese Sn-W deposits; Tectonic regime

1. Introduction

Northeast (NE) Vietnam has been considered as a southwestern continuation of the South China Block (SCB), based on their similar geological characteristics (Chen et al., 2014; Cheng et al., 2016; Mao et al., 2013, 2019, 2021). The Youjiang Basin (i.e. the Nanpanjiang Basin) is located to the southwest of the SCB and borders on NE Vietnam (Fig. 1B). Abundant Late Cretaceous Sn-W deposits, such as the Gejiu Sn-Cu, Bainiuchang Sn-Ag, Dulong Sn-Zn, Dachang Sn-Zn-Pb, and Damingshan W-Mo-Cu deposits, are distributed in the Youjiang Basin and its surrounding area (Fig. 1B). Recently, Sn-W deposits also have been found in NE Vietnam, which are commonly associated with late Mesozoic granitic intrusions, such as the Da Lien, Thien Ke, and PiaOac granites (Nguyen et al., 2019; Roger et al., 2012; Sanematsu and Ishihara, 2011; Vladimirov et al., 2012; Wang et al., 2011).

The Lung Muoi and Alexandra Sn-W deposits in the PiaOac area are famous Sn-W deposits in NE Vietnam. Petrological, geochronological and geochemical characteristics of the PiaOac granites have been investigated by some researchers (Chen et al., 2014; Nguyen et al., 2019; Roger et al., 2012; Vladimirov et al., 2012; Wang et al., 2011). However, the PiaOac granites have yielded a large range of crystallization ages varying from 94 Ma to 82 Ma, based on LA-ICPMS zircon U-Pb, SIMS zircon U-Pb, whole rock-mineral Rb-Sr isochrons and muscovite $^{39}Ar/^{40}Ar$ methods (Chen et al., 2014; Nguyen et al., 2019; Roger et al., 2012; Vladimirov et al., 2012; Wang et al., 2011). Does this span imply a long magmatic history, multi-stage magmatism or incorrect dating results? Furthermore, the

timing of Sn-W mineralization has not been constrained and the genetic relationship between the deposits and associated granites remains unclear. Therefore, the formation age and genetic relationships of the granites and associated Sn-W deposit in NE Vietnam require further constraints.

The granitic magmatism and associated Sn-W mineralization in NE Vietnam is spatially and temporally similar to those in SW SCB (Zhao et al., 2018). The magmatism and mineralization in both regions probably occurred in the same geodynamic setting (Chen et al., 2014; Cheng et al., 2016; Mao et al., 2019, 2021; Wang et al., 2011). However, the tectonic setting of Late Cretaceous granitic magmatism and related Sn-W mineralization in this area has not been fully understood. Some researchers described the Sn-W mineralization field in the SW SCB as a westward extension of the Nanling Metallogenic Belt in the central Cathaysia Block (Chen et al., 2015; Cheng and Mao, 2010), and suggested that the magmatism and related mineralization in the belt are controlled by the subduction and post-subduction of the Pacific Plate (Chen et al., 2015; Cheng et al., 2016; Mao et al., 2013, 2021; Zheng et al., 2017). Other scholars have proposed that they are probably related to the tectonic regime of the Neo-Tethys Ocean (Hu et al., 2020; Huang et al., 2019; Zhang et al., 2017, 2018, 2019).

This study provides new systematic LA-ICPMS zircon and cassiterite U-Pb geochronology, whole-rock geochemistry, and zircon Hf isotopic data for the PiaOac granites and associated deposits to constrain their age, petrogenesis, and tectonic setting. Combined with available data in NE Vietnam and SW South China, this paper sheds new light on the geodynamic implications of Late Cretaceous magmatism and related Sn-W mineralization in NE Vietnam and SW South China.

2. Regional geology and characteristics of the PiaOac granitic intrusion

2.1. Regional geology

Vietnam is geologically divided into five tectonic units from north to south, Northeast (NE) Vietnam, Northwest (NW) Vietnam, the Truong Son Belt, the Kontum Massif and the Nambo Block. NE Vietnam is composed of the Song Chay, Lo Gam, Quang Ninh, Song Hien, An Chau, and Ha Lang domains (Fig. 2A) (Tran and Vu, 2011).

This study focuses on the PiaOac granites in the Song Hien domain (Fig. 2B). The Song Hien domain is bordered by the Ha Lang domain to the east and the An Chau domain to the southeast. It consists mainly of Carboniferous to Triassic terrigenous - volcanic sequences (Hoa et al., 2008; Tran and Vu, 2011) (Fig. 2B). Magmatic activity is widely developed in the Song Hien domain. Permian-Triassic magmatic rocks include *ca* 274-262 Ma mafic-ultramafic rocks of the Cao Bang complex (Halpin et al., 2015; Hoa et al., 2008), 254-248 Ma rhyolites and dacites interbedded with volcano-sedimentary strata (Halpin et al., 2015; Hoa et al., 2008), and 252-245 Ma granites and granodiorites formed in a syn- to post-collisional setting (Chen et al., 2014; Halpin et al., 2015; Hoa et al., 2008; Roger et al., 2012). Late Cretaceous magmatic bodies are small and scattered, such as the PiaOac, Thien Ke, and Da Lien ones, representing the youngest magmatic rocks in the Song Hien domain. These Late Cretaceous granites are spatially associated with Sn-W deposits. These Sn-W deposits are magmatic-hydrothermal systems, including greisen-type mineralization and quartz vein-type mineralization mainly occurring in the upper parts of the two-mica granites (Fig. 1B) (Chen et al., 2014; Nguyen et al., 2019; Roger et al., 2012; Vladimirov et al., 2012; Wang et al., 2011).

2.2. Geology of the PiaOac intrusion

The PiaOac intrusion in NE Vietnam is located approximately 5 km southwest of Nguyen Binh Town, Cao Bang Province. It outcrops over an area about 3 km in width and 7 km in length (Fig. 2C).

The PiaOac intrusion is bounded by Early Devonian carbonate-terrigenous sedimentary rocks to the west and a Triassic volcanic-sedimentary sequence to the east. The former is composed mainly of schist and marble along the NW-SE trending fault, and the latter consists mainly of meta-rhyolite, mica quartz schist, meta-sandstone, and sericite shale (Fig. 2C). The economic deposits in the PiaOac region include the Alexandra Sn-W deposit in the north, the Lung Muoi Sn-W deposit in the east, and the CaoShon F-Be deposit in the northwest (Fig. 2C).

The Lung Muoi and Alexandra Sn-W deposits are mainly the greisen- and hydrothermal quartz-vein types. Quartz veins containing Sn-W minerals are the most important ore type. They are distributed in the greisen zone or greisenized granite (Fig. 4). Ore minerals in quartz veins and the greisen zone generally show no differences, but the Sn-W contents in quartz vein are higher than in greisen.

The Lung Muoi deposit has more than 100 ore-bearing quartz veins, with different orientations and thicknesses from 1cm to 30cm, sometimes up to 80cm. These ore-bearing quartz veins are concentrated in a northwest-southeast trending belt about 700m long with a width of 200-300m in the inner and outer zones of the PiaOac granite body. The Alexandr deposit has about 20 ore veins with thicknesses of 20–80cm and lengths of 50-400m. These ore veins are concentrated in a northwest-southeast extending zone 1500m long and 400m wide, which is distributed along the outer zone of the granite body.

In the Alexandra deposit, 4,665 metric tons of Sn-W ores with 1-2% $Sn+WO_3$ contents have been mined. The remaining resource is about 1,450 metric tons (Nguyen et al., 2009). In the Lung Muoi deposit, about 1,400 metric tons of Sn-W ore have been exploited, and the remaining resource is about 400 metric tons with ~1% $Sn+WO_3$ contents (Nguyen et al., 2009). The main ore minerals in the greisen zone and quartz vein include wolframite, cassiterite, molybdenite, chalcopyrite, sheelite, apatite, and pyrite.

The PiaOac intrusion consists mainly of medium- to coarse-grained two-mica granite and muscovite granite with minor aplite and pegmatite. The PiaOac granites are bright pink or yellowish and show massive structures and porphyritic textures with euhedral K-feldspar megacrysts (20-30%) up to 1-5 cm in length (Fig. 3A). Their main mineral assemblages are quartz (25-40%), K-feldspar (20-35%), plagioclase (20-25%), muscovite (3-7%), and biotite (1-3%) (Figs. 3C-F). Accessory minerals include ilmenite, apatite, beryl, monazite, zircon, and topaz. Detailed descriptions and locations of samples are listed in the Supplementary Table S1.

The PiaOac granites experienced different degrees of greisenization, especially at roof and contact zones with wall rocks. Greisenization leads to decomposition of feldspar and an increase in muscovite and quartz (Figs. 3D-F). The greisens consist mainly of quartz (55-70%) and muscovite (30-40%) with minor accessory minerals, such as fluorite, topaz, tourmaline, and zircon. The wolframite and cassiterite mineralization in the PiaOac area is commonly found in the greisens or greisenized granites (Figs. 4A, B), suggesting that the mineralization is closely related to hydrothermal alteration (Figs. 4A-D).

2.3. Paragenesis of the Sn-W deposits in the PiaOac area

In the Lung Muoi and Alexandra deposits (Fig. 2C), the main ore minerals, e.g. cassiterite and wolframite, are distributed in the greisen zone (Figs. 4A, B). A quartz-cassiterite-wolframite assemblage is the most common type of Sn-W mineralization in the PiaOac area. Ore-forming processes in the PiaOac area can be divided into 5 stages on the basis of mineral assemblages and reactions: stage 1 (weak alteration), stage 2 (greisenization), stage 3 (cassiterite-wolframite-tourmaline-quartz), stage 4 (cassiterite-quartz-sulfide), and stage 5 (quartz veins). The detailed mineral parageneses in different stages are described below and illustrated in Fig. 5.

Stage 1 (weak alteration): weak greisenization occurred in the granite and ore-forming minerals have not formed in this stage yet.

Stage 2 (greisenization): fluids and volatiles (such as F and S) of late magmatic evolution were brought to the arch of the granite pluton, and strong greisenization occurred there. Minor wolframite, cassiterite, molybdenite, and bismuth were formed in the greisen zone (Figs. 4A, B). Fluorite and apatite may have been formed in this stage (Figs. 4E, F).

Stage 3 (cassiterite-wolframite-tourmaline-quartz): cassiterite and wolframite are significantly enriched and accompanied by some other W-bearing minerals, such as sheelite and russelite (Figs. 4G-N). Cassiterite in the quartz veins is associated with tourmaline and molybdenite (Fig. 4C). Tourmaline in this stage can grow to larger crystals than those in stage 2 (Fig. 4C). Molybdenite in this stage is more abundant than that in stage 2.

Stage 4 (cassiterite-quartz-sulfide): the major ore minerals are cassiterite, wolframite, chalcopyrite, molybdenite, russellite, and pyrite, with minor bismuthinite (Figs. 4O-Q).

Stage 5 (quartz veins): mineral assemblages are dominated by quartz with minor pyrite and chalcopyrite (Fig. 4D).

3. Analytical methods

Zircon Cathodoluminescence (CL) imaging, U-Pb dating and Hf isotopic analyses, and cassiterite U-Pb dating analyses and backscattered electron images in this study were carried out at the State Key Laboratory for Mineral Deposits Research, Nanjing University, China. Major and trace element analyses were conducted at the ALS Minerals Laboratory (Guangzhou) Co Ltd, China. Details of all analytical instruments and processes are attached in Supporting information S1 file.

4. Analytical results

4.1. Zircon U-Pb dating and Hf isotopic results

Six representative samples from the PiaOac intrusion were selected for zircon U-Pb dating and Hf isotopic analyses, including three two-mica granite samples (PO 04-1, PO 06-1, and PO 06-2), two weakly greisenized granite samples (PO 07-1 and PO 08), and one greisen sample (PO 06-3). Zircon grains are mostly euhedral to subhedral and colorless, 50-200 μm in length and with aspect ratios of 3-1.5 (Fig. 6). Their CL images show clear oscillatory or parallel zoning with few inherited cores, suggesting a magmatic origin (Fernando et al., 2003; Hoskin and Black, 2000). Most zircon grains have low Th/U ratios (<0.4), which are caused by their extremely high U attributable to the high U contents of their host rocks. The zircon U-Pb dating and Hf isotopic results are listed in Tables S2 and S3, respectively.

LA-ICPMS zircon U-Pb dating results show that most zircons from the PiaOac two-mica granite, weakly greisenized granite, and greisen samples have concordant ages (concordance >90%), except for 5 grains in samples PO 04-1 and PO 06-1. These zircons yield similar $^{206}Pb/^{238}U$ ages ranging from 92 Ma to 85 Ma, except for two Triassic zircons in sample PO 06-1 (Table S2). Those discordant ages may be ascribed to the mixing of mineral inclusions with high common Pb in the grains. Only concordant zircons (concordance >90%) were used to calculate average ages. The weighted mean $^{206}Pb/^{238}U$ ages of six samples are 88.3 ± 1.3 Ma, 88.7 ± 0.7 Ma, 88.9 ± 0.8 Ma, 88.5 ± 0.7 Ma, 88.6 ± 0.7 Ma, and 88.2 ± 0.9 Ma, respectively (Fig. 7), indicating that the PiaOac granites were formed in Late Cretaceous time (89-88 Ma). Two zircon grains from sample PO 06-1 give $^{206}Pb/^{238}U$ ages of 238 Ma and 241 Ma, consistent with age of the nearby Triassic rhyolite, suggesting that these two zircon grains were captured from the rhyolite wall-rocks.

54 Late Cretaceous zircon grains from the six samples were further analyzed for Hf isotopic compositions. These zircons have initial $^{176}Hf/^{177}Hf$ values of 0.282274 to 0.282554, $\varepsilon_{Hf}(t)$ of -5.4 to -15.7, and two-stage Hf model ages (T_{DM}^2) of 1499-2144 Ma (Fig. 8; Table S3). Comparisons show that zircons from three granite samples have relatively homogeneous Hf isotopic compositions with variations of only 3.2 - 4.8 epsilon units, whereas the zircons from two weakly greisenized granites and one greisen show lower Hf isotopic compositions and larger variations with 5.7-6.4 epsilon units.

4.2. Cassiterite U-Pb dating results

Cassiterite grains were separated from two quartz vein samples (PO 06-4 and PO 07-4) in the Lung Muoi deposit and one sample (PO 09) in the Alexandra deposit. These cassiterite grains are dark yellow, light brown, or dark brown. They show oscillatory or banded zoning under CL (Figs. 6G-I). Their dating results are described in Table S4.

Thirty-two cassiterite grains were chosen for dating of each sample. They give similar $^{206}Pb/^{238}U$ ages ranging from 86.3 Ma to 92.7 Ma, 84.6 Ma to 92.6 Ma and 85.5 to 95.1 Ma for samples PO 06-4, PO 07-4 and PO 09, except a few grains. However, the ages of many grains are discordant with concordance <90%. These grains deviating from the Discordia line probably can be attributed to high common Pb. Only grains with concordance >90% were chosen to calculate a weighted mean age. The weighted mean ages of three samples are 88.8 ± 0.7 Ma, 88.6 ± 0.9 Ma and 88.9 ± 0.9 Ma respectively, identical with their lower intercept ages (Fig. 9). These data suggest that Sn mineralization in the two deposits is coeval (~89 Ma), and comparable to the zircon U-Pb ages of the PiaOac granite and greisen samples.

4.3. Major and trace elements of the PiaOac granites

The fresh and weakly greisenized granites (N-WAG) are characterized by high SiO_2 (70.3-74.3 wt.%), Na_2O (3.29-4.15 wt.%), and P_2O_5 (0.31-0.42 wt.%) with high A/CNK

(Al_2O_3/(CaO+Na_2O+K_2O) mole) (1.23-1.40), showing strongly peraluminous granite features (Table S5; Figs. 10A, B). They are enriched in K_2O relative to Na_2O and belong to the high K calc-alkaline series (Fig. 10C). The strongly greisenized granites and greisens (SGG-G) have lower Na_2O (0.14-1.90 wt.%) and higher A/CNK (1.24-2.40) than the N-WAG ones. The Harker diagram illustrates that $Fe_2O_3^T$ and MnO increased, and Na_2O and P_2O_5 decreased, during greisenization (Fig. 11).

All samples have low rare earth element (REE) concentrations (42.9-71.0 ppm). In the chondrite-normalized diagram (Fig. 12A), the N-WAG and SGG-G samples display similar REE patterns with light REE (LREE) enrichment relative to heavy REE (HREE) and significantly negative Eu anomalies. Both N-WAG and SGG-G do not exhibit significant tetrad effect with $TE_{1,3}$ = 1.08-1.12 (Fig. 12A; Table S5).

During greisenization, Li, Ga, Rb, Cs, and As significantly increased, whereas Be, Sr, Ba, Ta, and Pb decreased (Table S5). In the primitive mantle-normalized trace-element distribution diagram (Fig. 12B), the PiaOac granite and greisen samples are relatively enriched in Rb, Th, U, and Ta, and depleted in Ba, Sr, Nb, Ta, Eu, and Ti.

5. Discussion

5.1. Age and petrogenesis of the PiaOac granites

LA-ICPMS zircon U-Pb dating of six samples yielded ages of 88.2 Ma to 88.9 Ma (Fig. 7), interpreted as the ages of the PiaOac granites and greisens. Formation ages of the PiaOac granites were obtained previously using different methods, such as a SIMS zircon U-Pb age of 93.9 ± 3 Ma (Wang et al., 2011), SIMS zircon U-Pb ages of 90.6 ± 0.7 Ma and 90.1 ± 1.0 Ma (Chen et al., 2014), a LA-ICPMS zircon U-Pb age of 87.3 ± 1.2 Ma (Roger et al., 2012), LA-ICPMS zircon U-Pb ages of 82.5 ± 2.3 and 82 ± 1.8 Ma (Nguyen et al., 2019), a $^{87}Rb/^{86}Sr$ isochron age of 83.5 ± 6.2 Ma, and a muscovite $^{39}Ar/^{40}Ar$ age of 89.7 ± 1 Ma (Vladimirov et al., 2012). These dating results gave a wide

age range (94-82 Ma), and some of them have large errors. Our data concentrate at 89-88 Ma, similar to dating results of Chen et al. (2014), Roger et al. (2012) and Vladimirov et al. (2012). Wang et al. (2011) carried out U-Pb isotopic analyses of sixteen zircon grains from one sample, giving a large age range (189-86 Ma), except one older discordant age (678 Ma). However, they only chose nine intermediate values to yield a mean age of 93.9 ± 3.0 Ma with a large MSWD (4.9). As authors indicated that those old ages may be mixing ages, only the young ages should be used to calculate the real crystallization age of the magma. If the seven youngest concordant zircons are used, a more precise average age (90.4 ± 1.7 Ma) will be obtained with MSWD = 1.5. This age is similar to LA ICPMS zircon U-Pb ages in this study and the SIMS zircon U-Pb ages of Chen et al. (2014). On the other hand, the Rb-Sr isotope system generally has a lower closure temperature. Thus, the $^{87}Rb/^{86}Sr$ isochron age of 83.5 ± 6.2 Ma probably represents a cooling age. Therefore, we believed that the PiaOac granites and greisens most likely formed in the Late Cretaceous (90-87 Ma).

The PiaOac granites are characterized by aluminum-rich minerals such as muscovite (Fig. 3C) with a strongly peraluminous feature (A/CNK > 1.1) (Fig. 10), akin to S-type granite (Chappell, 1974; Chappell and White, 1992). Their Rb, Th, and Y variations also indicate the evolution trends of S-type granite (Fig. 13). On the other hand, the N-WAG samples are characterized by high SiO_2, K_2O, P_2O_5, K_2O/Na_2O, and Rb/Sr, different from those of highly differentiated I type granites (Whalen et al., 1987).

Geochemical data show that the PiaOac granites underwent strong fractional crystallization. On the diagram of $(Na_2O+K_2O)/CaO$ versus (Zr+Nb+Ce+Y) (Whalen et al., 1987), the PiaOac N-WAGs fall very near the fractionated granite field (Fig. 14). They have low Nb/Ta (2.6-3.5), K/Rb (39.9-64.6) and Zr/Hf (27.0-28.3), significantly lower than the average values of granites and primitive mantle (Fig. 15), indicating strong fractional crystallization. These features are consistent with their low Zr saturation temperatures (717-734^{O}C, Table S5) and the absence of inherited zircon cores (Fig.

6). On the Harker diagram (Fig. 11), the PiaOac granites show decreasing Al_2O_3 and K_2O with increasing SiO_2, indicating fractional crystallization of K-feldspar and/or biotite. Modeling calculations also indicate a clear trend of K-feldspar fractional crystallization (Fig. 16), and increasing $Fe_2O_3^T$, MgO, and TiO_2 rule out fractional crystallization of biotite. Therefore, the PiaOac granites underwent strong fractional crystallization of K-feldspar during the late evolution of the granitic magma. Compared with the Late Cretaceous granites in SW South China, the PiaOac granites have higher Na_2O+K_2O, P_2O_5 and silica, but lower Ca, Mg and Fe (Fig. 11). Moreover, the PiaOac N-WAG granites have higher Rb (average of 757 ppm) and lower Sr (~20 ppm) with higher Rb/Sr ratios (20.2-55.9) than most of the Late Cretaceous granites in SW South China (Fig. 12B, 17B; Table S5), suggesting different sources and degrees of differentiation among them.

The PiaOac two-mica granites (PO 04-1, PO 06-1, and PO 06-2) have concentrated zircon $\varepsilon_{Hf}(t)$ values of -9.5 to -8.7 and model ages (T_{DM}^2) of 1.71-1.76 Ga, similar to those of the Laojunshan and Bozhushan granites (Fig. 8), overlapping with the Hf-isotope compositions of Precambrian basement rocks in SW South China and NE Vietnam (SWSC-NEV) (Zhou et al.., 2018). Thus, the PiaOac granites were probably derived from a metasedimentary source with a late Paleoproterozoic model age, as also evidenced by their Nd-Sr-O isotopic data (initial $^{87}Sr/^{86}Sr$ ratio = 0.7251 to 0.7283, $\varepsilon_{Nd}(t)$ = -10.7 to -10.4, and $\delta^{18}O$ = 8.17 ‰ to 10.95 ‰; Chen et al., 2014; Wang et al., 2011). The low CaO/Na_2O, and high Rb/Ba and Rb/Sr ratios of the PiaOac N-WAGs further suggest a plagioclase-poor and clay-rich pelitic source (Fig. 17; Sylvester, 1998).

5.2. Age and genesis of the Sn-W mineralization

In this study, LA-ICPMS U-Pb dating of cassiterite is used for the first time to determine the mineralization age of the Sn-W deposits in the PiaOac region. The dating results for three samples from the Lung Muoi and Alexandra deposits show that the Sn-W mineralization occurred at ~89 Ma, coincident with the crystallization of the PiaOac granites. Therefore, the Sn-W mineralization in the

PiaOac region is closely related to the PiaOac granites, which is also supported by their highly fractionated geochemical characteristics (Fig. 14, 15).

Zircon Hf-isotope analyses show that the PiaOac greisen (PO 06-3) has significantly low zircon Hf-isotope compositions with average $\varepsilon_{Hf}(t)$ of -12.2 and a larger range of Hf-isotope variation (Table S3). Zircons from two weakly greisenized granites (PO 07-1 and PO 08) also show larger Hf-isotope variations than those from two-mica granites, and slightly lower $\varepsilon_{Hf}(t)$ values (-9.2 and -9.6) (Fig. 8; Table S3). These observations suggest that the greisenization led to significant changes of not only whole rock major- and trace elements but also zircon Hf-isotope composition. More enriched Hf-isotope compositions of the greisen are probably caused by strong interaction with wall rocks due to fluid-rich environment at final stage of magmatic evolution. The interaction of fluid-rich residual magma with wall rocks was probably an important mechanism resulting in the change of redox environment, which was favorable for the W-Sn mineralization (Nguyen et al., 2019).

5.3. Tectonic setting of Late Cretaceous magmatism and mineralization in NE Vietnam and SW South China

In addition to the PiaOac granite, other Late Cretaceous granites have been recognized in NE Vietnam, e.g. the DaLien granite (86-81 Ma; Nguyen et al., 2020; Sanematsu and Ishihara, 2011). Extensive Late Cretaceous granites have also been found in SW South China, such as the Gejiu (87-77 Ma), Bozhushan (88-85 Ma), Laojunshan (93-83 Ma), Dachang (97-91 Ma), and Damingshan (97-93 Ma) granites (Fig. 18A). Except for the Dachang and Damingshan granites, other Late Cretaceous granites predominantly mainly formed over a short time span (89-83 Ma), coincident with the 90-81 Ma granites in NE Vietnam. Coeval deposits were also identified in SW South China, as exemplified by the 86-83 Ma Gejiu Sn-Cu, 88-87 Ma Bainiuchang Sn-Ag, 96-75 Ma Dulong Sn-W, 95-90 Ma Dachang Sn-Zn-Pb, and 99-94 Ma Damingshan W-Mo-Cu deposits. It is suggested that the

mineralization is temporally and spatially related to the Late Cretaceous granitic magmatism in SW South China and NE Vietnam (SWSC-NEV).

NE Vietnam not only has the same Late Cretaceous magmatism and mineralization as SW South China, but also has similar Precambrian basement (Zhou et al., 2018). NE Vietnam is probably the southwestern extension of SW South China, and belongs to the same metallogenic domain, i.e. the Late Cretaceous SWSC-NEV metallogenic belt. In fact, this metallogenic belt may extend eastward to western Guangdong Province (Fig. 1A; Hu et al., 2020; Zhang et al., 2018, 2019; Zheng et al., 2017). The Sn-W mineralization in South China is world famous and mainly occurred in Late Jurassic time (165-150 Ma) along the E-W Nanling Range of the central Cathaysia Block (Hua et al., 2005; Mao et al., 2007). The SWSC-NEV Sn-W metallogenic belt spatially and temporally does not match with the Nanling W-Sn metallogenic belt (Fig. 1A), and consequently is not the western extension of the Nanling W-Sn metallogenic belt (Chen et al., 2015; Cheng et al., 2010). They should be formed in different tectonic regime.

The tectonic setting of the Late Cretaceous magmatism and mineralization in the SWSC-NEV belt has been controversial. Some researchers believe that the Late Cretaceous magmatism and mineralization are related to the subduction of the Paleo-Pacific plate beneath the Eurasian continent (Chen et al., 2015; Cheng et al., 2008, 2016; Mao et al., 2013, 2021; Zheng et al., 2017), whereas other geologists have proposed that these processes were related to the subduction of the Neo-Tethys plate (Hu et al., 2020; Huang et al., 2019; Yang et al., 2020; Zhang et al., 2018, 2019). In addition, a few scholars have ascribed the formation of these granites and deposits to the subduction regimes of both Paleo-Pacific and Neo-Tethys plates (Wang et al., 2011).

Those holding the first opinion have correlated the Late Cretaceous magmatic activity in the SWSC-NEV belt with those on the southeastern coast of South China, and proposed that they were induced by the subduction of the Paleo-Pacific Plate beneath the Eurasian continent (Cheng et al.,

2016; Mao et al., 2013, 2021; Roger et al., 2012). The Late Cretaceous magmatic rocks along the southeastern coast are high-K calc-alkaline I-type granites, A-type granites, I- and A- type composite complexes, or bimodal volcanic rocks, with a paucity of Sn-W mineralization (Martin et al., 1994; Qiu et al., 2008; Zhou and Li, 2000; Zhou et al., 2006), different from those in the SWSC-NEV belt, which is dominated by numerous small S-type granitic bodies associated with abundant Sn-W deposits and less Cu deposits (Huang et al., 2019 and references therein). The southeastern coast experienced multistage and long-lasting late Mesozoic magmatic activity from 146 Ma to 87 Ma (Li, 2000; Zhou and Li, 2000; Zhou et al., 2006), predating the magmatic activity in the SWSC-NEV belt (Fig. 18). Furthermore, the E-W trend of the SWSC-NEV belt seems inconsistent with the northwestward subduction of the Paleo-Pacific Plate.

On the other hand, the granites in the SWSC-NEV belt mostly belong to highly fractionated S-type granites (Figs. 10, 14, 15). In the discrimination diagrams of tectonic setting, they mostly fall into the fields of syn- to post-collisional granite (Fig. 19), except for those in western Guangdong Province, at the eastern extremity of the SWSC-NEV belt. No Late Cretaceous volcanic arc-related granites and mafic rocks have been identified in the SWSC-NEV belt. A few alkaline mafic to intermediate rocks in the Gejiu area were considered to form in post-orogenic extensional setting (Huang et al., 2016). These observations suggest that the Late Cretaceous magmatism and mineralization in the SWSC-NEV belt were different from typical subduction-related magmatism and metallogeny along the East Asian continent margin, implying that it is far from the ocean subduction zone and probably formed in an intracontinental orogenic setting.

Similarly, there is no conclusive evidence related to the subduction of the Neo-Tethys Ocean in the study area. The SWSC-NEV belt is also far from the western Myanmar - Tengchong metallogenic domain, where the magmatism and metallogeny have been demonstrated to be closely related with the subduction of the Neo-Tethys Ocean (Mao et al., 2019, 2021). Consequently, based on its special

tectonic position between the Pacific and Tethys tectonic regimes, and characteristics of Late Cretaceous magmatism and metallogeny in the SWSC-NEV belt, it is suggested that the belt probably resulted from the far-field effect of the Pacific and Tethys tectonic regimes together.

6. Conclusions

(1) The PiaOac granites formed at 90-87 Ma, and associated Sn-W mineralization occurred at ~89 Ma, indicating that the Sn-W mineralization in NE Vietnam was closely related to the granitic magmatism.

(2) The whole-rock geochemical and zircon Hf isotopic compositions indicate that the PiaOac intrusions are strongly peraluminous and highly fractionated S-type granites, which were derived from partial melting of metasedimentary rocks with late Paleoproterozoic model ages. Zircon Hf-isotope compositions are more enriched from granite to greisen, suggesting strong interaction of highly differentiatied magma with wall rocks in the late fluid-rich stage, which modified not only trace element and Hf-isotope compositions but also the redox environment, and consequently facilitated the Sn-W precipitation.

(3) The PiaOac granites and associated Sn-W mineralization in NE Vietnam are similar to those in SW South China in terms of geochronological and geochemical characteristics, source compositions, deposit type, and tectonic setting, all together constituting the SWSC-NEV Late Cretaceous metallogeny belt.

(4) The Late Cretaceous magmatism and metallogeny in the SWSC-NEV belt are not spatially and temporally related to the Late Jurassic granitic magmatism and W-Sn metallogeny in the Nanling Range, central Cathaysia Block, nor the Late Cretaceous magmatism and metallogeny along the southeastern coast of South China. The Late Cretaceous granites and associated deposits in the SWSC-NEV belt

probably were formed in an intracotinental orogenic setting, which resulted from the combined action of Pacific and Neo-Tethys tectonic regimes.

Acknowledgements

This work was supported by the NSF of China (grant no. 91962221) and the National Key Research and Development Program of China (2016YFC0600204). We thank Dr. NgocThai Tran, Prof. Liangshu Shu and Prof. Jianjun Lu for their help in the fieldwork, and thank Professor W.L. Griffin for polishing the English of this article.

References

Ballouard, C., Poujol, M., Boulvais, P., Branquet, Y., Tartèse, R., Vigneresse, J.L., 2016. Nb-Ta fractionation in peraluminous granites: A marker of the magmatic-hydrothermal transition. Geology 44 (3), 231-234.

Bui, T. H., Nguyen, D. T., Trinh, D. H., Nguyen, V. N., Nguyen, V. S., Hoang, V. D., Nguyen, T. T., 2009. Investigation and assessment of tin - tungsten ore in Pia Oac area, Nguyen Binh district, Cao Bang province. Archived at the Geological Division for Radioactive And Rare Elements, Hanoi, (in Vietnamese).

Chappell, B.W., 1974. Two contrasting granite types. Pacific Geology 8, 173-174.

Chappell, B.W., 1999. Aluminium saturation in I- and S-type granites and the characterization of fractionated haplogranites. Lithos 46 (3), 535-551.

Chappell, B.W., White, A.J.R., 1992. I- and S-type granites in the Lachlan Fold Belt. Earth Sci 83, 1-26.

Chen, X.C., Hu, R.Z., Bi, X.W., Zhong, H., Lan, J.B., Zhao, C.H., Zhu, J.J., 2015. Zircon U-Pb ages and Hf-O isotopes, and whole-rock Sr–Nd isotopes of the Bozhushan granite, Yunnan province, SW China: Constraints on petrogenesis and tectonic setting. Journal of Asian Earth Sciences 99, 57-71.

Chen, Z.C., Lin, W., Faure, M., Lepvrier, C., Nguyen, V.V., Vu, V.T., 2014. Geochronology and isotope analysis of the Late Paleozoic to Mesozoic granitoids from northeastern Vietnam and implications for the evolution of the South China block. Journal of Asian Earth Sciences 86, 131-150.

Cheng, Y.B., Mao, J.W., 2010. Age and geochemistry of granites in Gejiu area, Yunnan province, SW China: Constraints on their petrogenesis and tectonic setting. Lithos 120, 258-276.

Cheng, Y.B., Mao, J.W., Chen, X.L., Li, W., 2010. LA-ICP-MS Zircon U-Pb Dating of the Bozhushan Granite in Southeastern Yunnan Province and Its Significance. Journal of Jilin University (Earth Science Edition) 40, 869-878.

Cheng, Y.B., Mao, J.W., Liu, P., 2016. Geodynamic setting of Late Cretaceous Sn-W mineralization in southeastern Yunnan and northeastern Vietnam. Solid Earth Sciences 1, 79-88.

Cheng, Y.B., Mao, J.W., Spandler, C., 2013. Petrogenesis and geodynamic implications of the Gejiu igneous complex in the western Cathaysia block, South China. Lithos 175, 213-229.

Cheng, Y. B., Mao, J. W., Xie, G. Q., Chen, M. H., Zhao, C. S., Yang, Z. X., Zhao, H. J., Li, X. Q., 2008. Petrogenesis of the Laochang-Kafang Granite in the Gejiu Area, Yunnan Province: Constraints from Geochemistry and Zircon U-Pb Dating. Acta Petrologica Sinica 82 (11), 1478-1493.

Feng, J.R., Mao, J.W., Pei, R.F., 2013. Ages and geochemistry of Laojunshan granites in southeastern Yunnan, China: implications for W-Sn polymetallic ore deposits. Mineralogy Petrology 107 (4), 573-589 (in Chinese with English abstract).

Fernando, C., John, M.H., Paul, W.O.H., Peter, K., 2003. Atlas of Zircon Textures. Reviews in Mineralogy and Geochemistry 53 (1), 469-500.

Guo, J., Zhang, R.Q., Sun, W.D., Ling, M.X., Hu, Y.B., Wu, K., Luo, M., Zhang, L.C., 2018b. Genesis of tin-dominant polymetallic deposits in the Dachang district, South China: Insights from cassiterite U-Pb ages and trace element compositions. Ore Geology Reviews 95, 863-879.

Halpin, J.A., Tran, H.T., Lai, C.K., Meffre, S., Crawford, A.J., Zaw, K., 2015. U-Pb zircon geochronology and geochemistry from NE Vietnam: A 'tectonically disputed' territory between the Indochina and South China blocks. Gondwana Research 34, 254-273.

Harris, N.B., Pearce, J.A., Tindle, A.G., 1986. Geochemical characteristics of collision-zone magmatism. Geological Society, London, Special Publications 19 (1), 67-81.

Hilde, T.W.C., Uyeda, S., Kroenke, L., 1977. Evolution of the western pacific and its margin. Tectonophysics 38 (1), 145-165.

Hoa, T.T., Izokh, A.E., Polyakov, G.V., Borisenko, A.S., Anh, T.T., Balykin, P.A., Phuong, N.T., Rudnev, S.N., Van, V.V., Nien, B.A., 2008. Permo-Triassic magmatism and metallogeny of Northern Vietnam in relation to the Emeishan plume. Russian Geology and Geophysics 49 (7), 480-491.

Hoskin, P.W.O., Black, L.P., 2000. Metamorphic zircon formation by solid-tate recrystallization of protolith igneous zircon. Journal of Metamorphic Geology 18 (4), 423-439.

Hu, P.C., Zhu, W.G., Zhong, H., Zhang, R., Zhao, X.Y., Mao, W., 2020. Late Cretaceous granitic magmatism and Sn mineralization in the giant Yinyan porphyry tin deposit, South China: constraints from zircon and cassiterite U–Pb and molybdenite Re–Os geochronology: Mineralium Deposita, 1-23.

Hua, R., Chen, P., Zhang, W., Yao, J., Lin, J., Zhang, Z., Gu, S., Liu, X., Qi, H., 2005. Metallogenesis related to Mesozoic granitoids in the Nanling Range, South China and their geodynamic settings. Acta Geologica Sinica (English Edition) 79, 810–820.

Huang, W.T., Liang, H.Y., Zhang, J., Wu, J., Chen, X.L., Ren, L., 2019. Genesis of the Dachang Sn-polymetallic and Baoshan Cu ore deposits, and formation of a Cretaceous Sn-Cu ore belt from southwest China to western Myanmar. Ore Geology Reviews 112, 103030.

Huang, W.L., Xu, J.F., Chen, J.L., Huang, F., Zeng, Y.C., Pi, Q.H., Cai, Y.F., Jiang, X.Z., 2016. Geochronology and grochemistry of the Gejiu complex in the Yunnan Province, SW China: Petrogenesis and contributions of mantle-derived melts to tin mineralization. Acta Petrologica Sinica 32, 2330-2346 (in Chinese with English abstract).

Lepvrier, C., Faure, M., Van, V.N., Vu, T.V., Lin, W., Trong, T.T., Hoa, P.T., 2011. North-directed Triassic nappes in Northeastern Vietnam (East Bac Bo). Journal of Asian Earth Sciences 41 (1), 56-68.

Li, J.H., Zhang, Y.Q, Dong, S.W., Johnston, S.T. 2014. Cretaceous tectonic evolution of South China: A preliminary synthesis. Earth Science Reviews 134, 98-136.

Li, X-H., 2000. Cretaceous magmatism and lithospheric extension in Southeast China. Journal of Asian Earth Sciences 18, 293-305.

Maniar, P.D., Piccoli, P.M., 1989.Tectonic discrimination of granitoids. GSA Bullet 101(5), 635-643.

Mao, J.W., Xie, G.Q., Guo, C.L., 2007. Large-scale tungsten-tin mineralization in the Nanling region, South China: metallogenic ages and corresponding geodynamic processes. Acta Petrologica Sinica 23, 2329-2338 (in Chinese with English abstract).

Mao, J.W., Cheng, Y.B., Chen, M.H., Franco, P., 2013. Major types and time–space distribution of Mesozoic ore deposits in South China and their geodynamic settings. Mineralium Deposita 48 (3), 267-294.

Mao, J.W., Ouyang, H.G., Song, S.W., Santosh, M., Yuan, S.D., Zhou, Z.H., Zheng, W., Li, H., Liu, P., Cheng, Y.B., Chen, M.H., 2019. Geology and metallogeny of tungsten and tin deposits in China. Soc. Econ. Geol. Special Publ. 22, 411- 482.

Mao, J.W., Liu, P., Goldfarb, R. J., Goryachev, N. A., Pirajno, F., Zheng, W., Zhou, M.F., Zhao, C., Xie, G.Q., Yuan, S.D., Liu, M., 2021. Cretaceous large-scale metal accumulation triggered by post-subductional large-scale extension, East Asia. Ore Geology Reviews 136, 104270.

Martin, H., Bonin, B., Capdevila, R., Jahn, B.M., Lameyre, J., Wang, Y., 1994. The Kuiqi peralkaline granitic complex (SE China): petrology and geochemistry. Journal of Petrology 35 (4), 983-1015.

Middlemost, E.A.K., 1994. Naming materials in the magma/igneous rock system. Earth-Science Reviews 37 (3), 215-224.

Nguyen, T.A., Y, Y.X., Vu, H.T., Liu, L., Lee, I.S., 2019. Piaoac granites related W-Sn mineralization, Northern Vietnam: evidences from geochemistry, zircon geochronology and Hf isotopes. Journal of Earth Science 30 (1), 52-69.

Nguyen, T. H., Nevolko, P. A., Pham, T. D., Svetlitskaya, T. V., Tran, T. H., Shelepaev, R. A., Fominykh, P. A., Pham, N. C., 2020. Age and genesis of the W-Bi-Cu-F (Au) Nui Phao deposit, Northeast Vietnam: Constrains from U-Pb and Ar-Ar geochronology, fluid inclusions study, S-O isotope systematic and scheelite geochemistry. Ore Geology Reviews 123, 103578.

Pearce, J.A., Harris, N.B.W., Tindle, A.G., 1984. Trace element discrimination diagrams for the tectonic interpretation of granitic rocks. Journal of Petrology 25 (4), 956-983.

Peccerillo, A., Taylor, S.R., 1976. Geochemistry of eocene calc-alkaline volcanic rocks from the Kastamonu area, Northern Turkey. Contributions to Mineralogy Petrology 58 (1), 63-81.

Qiu, J.S., Xiao, E., Hu, J., Xu, X.S., Jiang, S.Y., Li, Z., 2008. Petrogenesis of highly fractionated I-type granites in the coastal area of northeastern Fujian Province: constraints from zircon U-Pb geochronology, geochemistry and Nd-Hf isotopes. Acta Petrologica Sinica 24, 2468-2484 (in Chinese with English abstract).

Roger, F., Maluski, H., Lepvrier, C., Vu, V.T., Paquette, J.L., 2012. LA-ICPMS zircons U/Pb dating of Permo-Triassic and Cretaceous magmatisms in Northern Vietnam-Geodynamical implications. Journal of Asian Earth Sciences 48, 72-82.

Sanematsu, K., Ishihara, S., 2011. $^{40}Ar/^{39}Ar$ ages of the Da Lien granite related to the Nui Phao W mineralization in Northern Vietnam. Resource Geology 61 (3), 304-310.

Stern, R.J., Bloomer, S.H., 1992. Subduction zone infancy: examples from the Eocene Izu-Bonin-Mariana and Jurassic California arcs. Geological Society of America Bulletin 104 (12), 1621-1636.

Sun, S.S., McDonough, W.F., 1989. Chemical and isotopic systematics of oceanic basalts: implications for mantle composition and processes. Geological Society London Special Publications 42 (1), 313-345.

Sylvester, P.J., 1998. Post-collisional strongly peraluminous granites. Lithos 45 (1), 29-44.

Tran, V.T., Vu, K., 2011. Geology and Earth Resources of Vietnam. General Dept of Geology and Minerals of Vietnam. Publishing House for Science and Technology, Hanoi, 645.

Vladimirov, A.G., Phan, L.A., Kruk, N.N., Smirnov, C.Z., Annikova, I.Y., Pavlova, G.G., Kuibida, M.L., Moroz, E.N., Sokolova, E.N., Astrelina, E.I., 2012. Petrology of the tin-bearing granite-leucogranites of the Piaoak Massif, Northern Vietnam. Petrology 20 (6), 545-566.

Wang, D.S., Liu, J.L., Tran, M.D., Nguyen, Q.L., Guo, Q., Wu, W.B., Zhang, Z.C., Zhao, Z.D., 2011. Geochronology, geochemistry and tectonic significance of granites in the Tinh Tuc W-Sn ore deposits, Northeast Vietnam. Acta Petrologica Sinica 27 (9), 2795-2808 (in Chinese with English abstract).

Wang, J., Peng, L., Xu, Y., Zhang, N., Li, G., 2015. Types and correction methods of matrix effect during zircon LA-ICPMS U-Pb dating. Acta Geologica Sinica 89 (6), 2099-2100.

Wang, Q., Li, J.W., Jian, P., Zhao, Z.H., Xiong, X.L., Bao, Z.W., Xu, J.F., Li, C.F., Ma, J.L., 2005. Alkaline syenites in eastern Cathaysia (South China): Link to Permian-Triassic transtension. Earth and Planetary Science Letters 230, 339-354.

Wang, T., Li, G., Wang, Q., Santosh, M., Zhang, Q., Deng, J., 2019. Petrogenesis and metallogenic implications of Late Cretaceous I- and S-type granites in Dachang-Kunlunguan ore belt, southwestern South China Block. Ore Geology Reviews 113, 103079.

Whalen, J.B., Currie, K.L., Chappell, B.W., 1987. A-type granites: geochemical characteristics, discrimination and petrogenesis. Contributions to Mineralogy and Petrology 95 (4), 407-419.

Xu, B., Jiang, S.Y., Wang, R., Ma, L., Zhao, K.D., Yan, X., 2015. Late Cretaceous granites from the giant Dulong Sn-polymetallic ore district in Yunnan Province, South China: Geochronology, geochemistry, mineral chemistry and Nd-Hf isotopic compositions. Lithos 218, 54-72.

Yang, G-S., Wen, H., Ren, T., Xu, S., Wang, C., 2020. Geochronology, geochemistry and Hf isotopic composition of Late Cretaceous Laojunshan granites in the western Cathaysia block of South China and their metallogenic and tectonic implications. Ore Geology Reviews 117, 103297.

Zhang, L., Zhang, R., Hu, Y., Liang, J., Ouyang, Z., He, J., Chen, Y., Guo, J., Sun, W., 2017. The formation of the Late Cretaceous Xishan Sn-W deposit, South China: Geochronological and geochemical perspectives. Lithos 290‐291, 253‐268.

Zhang, L., Zhang, R., Wu, K., Chen, Y., Li, C., Hu, Y., He, J., Liang, J., Sun, W., 2018. Late Cretaceous granitic magmatism and mineralization in the Yingwuling W-Sn deposit, South China: constraints from zircon and cassiterite U-Pb geochronology and wholerock geochemistry. Ore Geology Reviews 96, 115−129.

Zhang, L., Zhang, R., Chen, Y., Sun, S., Liang, J., Sun, W., 2019. Geochronology and geochemistry of the Late Cretaceous Xinpeng granitic intrusion, South China: Implication for Sn-W mineralization. Ore Geology Reviews 113, 103075.

Zhao, Z.Y., Hou, L., Ding, J., Zhang, Q.M., Wu, S.Y., 2018. A genetic link between Late Cretaceous granitic magmatism and Sn mineralization in the southwestern South China Block: A case study of the Dulong Sn-dominant polymetallic deposit. Ore Geology Reviews 93, 268-289.

Zheng, W., Mao, J.W., Zhao, H.J., Ouyang, H.G., Zhao, C.S., Yu, X.F., 2017. Geochemistry, Sr–Nd–Pb–Hf isotopes systematics and geochronological constrains on petrogenesis of the Xishan A-type granite and associated W–Sn mineralization in Guangdong Province, South China. Ore Geology Reviews 88, 739-752.

Zhou, X.Y., Yu, J.-H., O'Reilly, S.Y., Griffin, W.L., Sun, T., Wang, X., Tran, M., Nguyen, D., 2018. Component variation in the late Neoproterozoic to Cambrian sedimentary rocks of SW China – NE Vietnam, and its tectonic significance. Precambrian Research 308, 92-110.

Zhou, X.M., Li, W.X., 2000. Origin of Late Mesozoic igneous rocks in Southeastern China: implications for lithosphere subduction and underplating of mafic magmas. Tectonophysics 326 (3), 269-287.

Zhou, X.M., Sun, T., Shen, W.Z., Shu, L.S., Niu, Y., 2006. Petrogenesis of Mesozoic granitoids and volcanic rocks in South China: A Response to Tectonic Evolution. Episodes 29, 26-33.

Figure captions

Fig.1: (A) Tectonic units of Southeast Asia and the location of the studied area. The SWSC-NEV belt represents the Late Cretaceous magmatism and metallogenic belt in SW South China and NE Vietnam; (B) Geological sketch map showing the distribution of Late Cretaceous intrusive rocks and associated Sn-W deposits in NE Vietnam and SW South China (modified from Cheng et al., 2013; Guo et al., 2018; Wang et al., 2005).

Fig. 2. (A) Simplified tectonic domains of North Vietnam (Hoa et al., 2008); (B) Geological map of the Song Hien domain and adjacent regions (modified from Lepvrier et al., 2011); (C) Geological map of the PiaOac district showing sample locations (after Nguyen et al., 2019).

Fig. 3. Field photographs and photomicrographs of the PiaOac granites: (A) PiaOac granite; (B) PiaOac granites intruding Triassic rhyolite; (C) two-mica granite; (D and E) greisenized granite; (F) greisen; Kfs – K-feldspar, Qz - quartz, Bt - biotite, Pl - plagioclase, Mus - muscovite, Brl - beryl, Cst - cassiterite.

Fig. 4. Photographs and BSE images of the Sn-W ores in the PiaOac area: (A and B) Wolframite-cassiterite-molybdenite in the greisenized granite; (C) Cassiterite-wolframite-molybdenite-tourmaline bearing quartz veins; (D) quartz veins cutting greisenized granite; (E and F) mineralization in greisen zone; (G-Q) mineralization in quartz veins; Cst - cassiterite; Wof -wolframite; Rus - russellite; Bm - bismuth; Bmt - bismuthinite; She - sheelite; Py - pyrite; Mo - molybdenite; Tur - tourmaline, Ap - apatite; Mus - Muscovite; Fl - fluorite; Qz - quartz.

Fig. 5. Parageneses of multiple mineralization stages in the Lung Muoi and Alexandra Sn-W deposits.

Mineral abbreviations are the same as those in Fig. 4.

Fig. 6. (A-F) Zircon cathodoluminescence (CL) images with dating (small circles) and Hf-isotope analytical spots (large circles). (G-I) CL images of representative cassiterite grains.

Fig. 7. U-Pb concordia diagrams of the zircon grains from the PiaOac granites and greisens.

Fig. 8. Plot of zircon $\varepsilon_{Hf}(t)$ versus U-Pb age. Data sources: the PiaOac granite (this study; Chen et al., 2014; Nguyen et al., 2019), the Laojunshan granite (Xu et al., 2015, Zhao et al., 2018), the Bozhushan granite (Chen et al., 2015), the Gejiu granite (Cheng and Mao 2010) and the Dachang granite (Wang et al., 2019).

Fig. 9. U-Pb concordia diagrams of cassiterite grains and weighted mean $^{206}Pb/^{238}U$ ages for the Lung Muoi and Alexandra Sn-W deposits. (A and B) samples PO 06-4 and PO 07-4 from Lung Muoi deposit, (C) sample PO 09 from Alexandra deposit.

Fig. 10. (A) SiO_2 *vs* (Na_2O+K_2O) diagram (after Middlemost, 1994); (B) diagram of $Al_2O_3/(CaO+Na_2O+K_2O)$ (mol) *vs* $Al_2O_3/(Na_2O+K_2O)$ (mol) (after Maniar and Piccoli (1989)); (C) SiO_2 *vs* K_2O diagram (after Peccerillo and Taylor (1976)). Data sources: PiaOac granite (this study; Nguyen et al., 2019; Wang et al., 2011), the Laojunshan granite (Feng et al., 2013, Xu et al., 2015, Zhao et al., 2018), the Bozhushan granite (Chen et al., 2015), the Gejiu granite (Cheng and Mao, 2010) and the Dachang granite (Wang et al., 2019).

Fig. 11. Harker diagrams of the PiaOac granites and greisens and other Late Cretaceous granites in SW South China. Data sources are the same as those cited in Fig. 10.

Fig. 12. (A) Chondrite-normalized rare earth element patterns. (B) Spider diagrams of primitive mantle-normalized trace element distributions for the PiaOac granites and the Late Cretaceous granites in SW South China. The normalization values are from Sun and McDonough (1989). Reference data are the same as those cited in Fig. 10.

Fig. 13. Diagrams of Rb *vs* Th (A) and Y (B) (after Chappell (1999)). Data sources are the same as those cited in Fig. 10.

Fig. 14. (K_2O+Na_2O)/CaO *vs* Zr+Nb+Ce+Y diagram (after Whalen et al. (1987)). Data sources are the same as those cited in Fig. 10.

Fig. 15. Nb/Ta *vs* Zr/Hf plot showing the relationship between the magma differentiation degree and mineralization (after Ballouard et al., 2016). Data sources are the same as those cited in Fig. 10.

Fig. 16. Fractional crystallization modeling for the PiaOac granites and Late Cretaceous granites in SW South China (after Cheng and Mao (2010)). Cpx - clinopyroxene, Opx - orthopyroxene, Pl - plagioclase, Kf - K-feldspar, Bi – biotite. Data sources as those in Fig. 10.

Fig. 17. CaO/Na_2O *vs* Al_2O_3/TiO_2 (A) and Rb/Ba *vs* Rb/Sr (B) diagrams (after Sylvester (1998)). Data sources are the same as those cited in Fig. 10.

Fig. 18. Geochronology framework of the Late Cretaceous granites (A) and Sn-W deposits (B) in the SWSC-NEV belt. Age data are compiled in the database (Table S6).

Fig. 19. Discrimination diagrams of tectonic setting for Late Cretaceous granites in the SWSC-NEV belt (after Harris et al., 1986; Pearce et al., 1984). WPG: Within-plate granite; VAG: Volcanic arc granite; syn-COLG: Syn-collisional granite; ORG: Ocean ridge granite. Reference are from those cited in Fig. 10.

Highlights:

PiaOac granites and associated Sn-W deposits in NE Vietnam formed in Late Cretaceous (89-87 Ma);

Magmatism and mineralization in NE Vietnam are similar to those in SW South China;

This Late Cretaceous Sn-W metallogeny belt is different from the Nanling metallogeny belt;

The belt resulted from the combined action of subduction of the Pacific and Neo-Tethys plates.

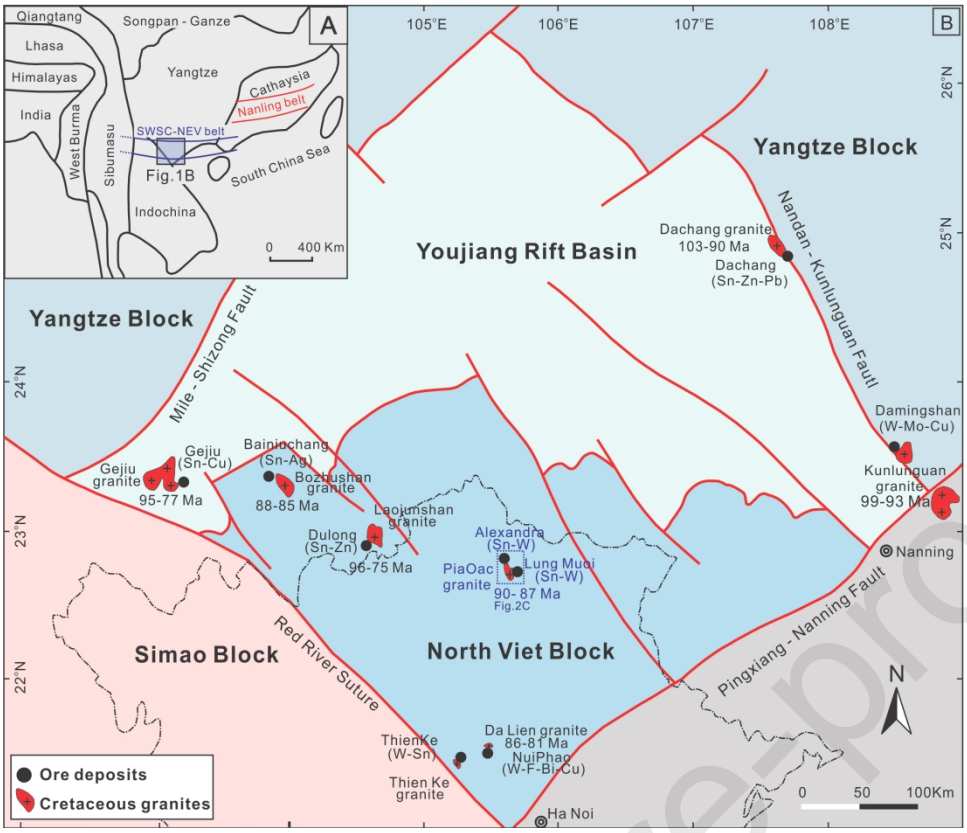

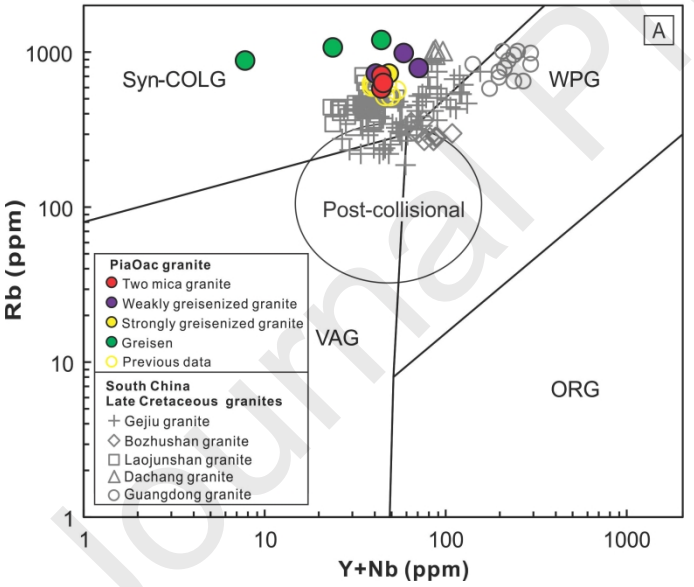

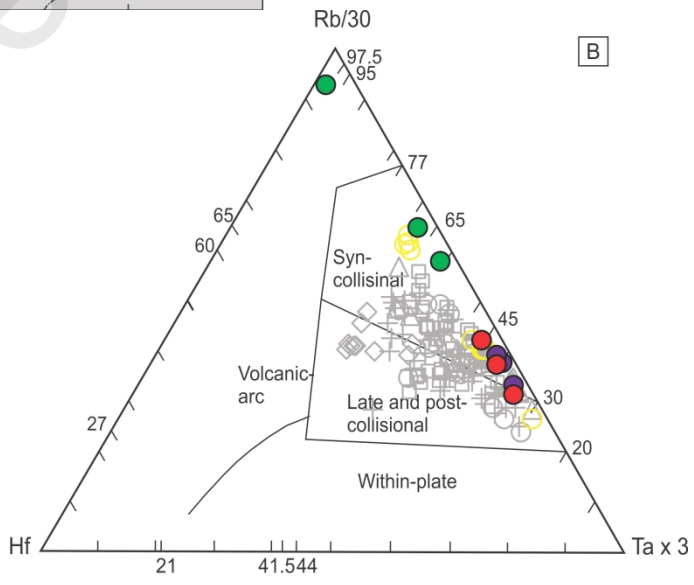

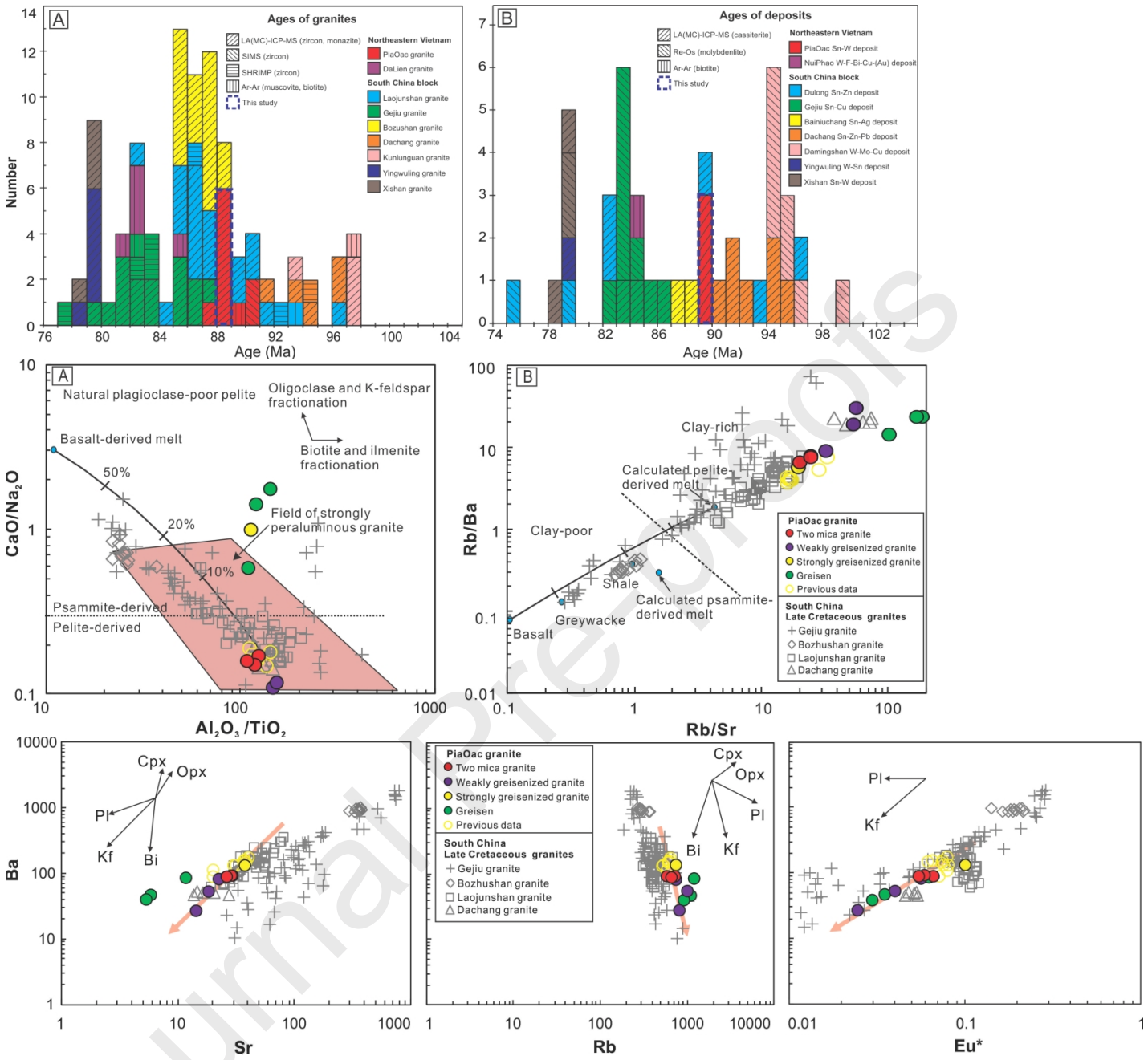

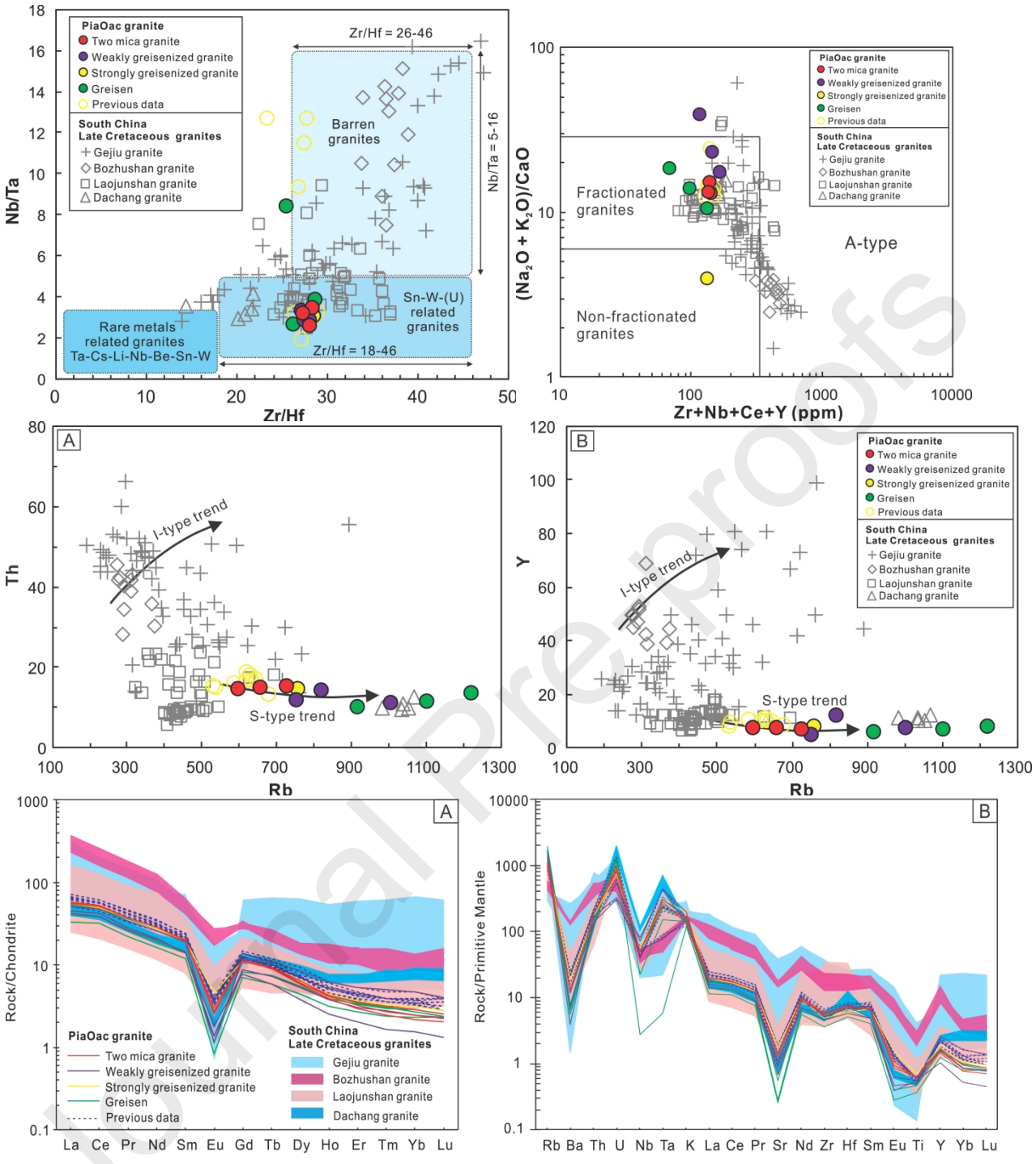
PiaOac granite
Two mica granite
Weakly greisenized granite
Strongly greisenized granite
Greisen
Previous data
South China
Late Cretaceous granites
Gejiu granite
Bozhushan granite
Laojunshan granite
Dachang granite
Zr/Hf = 26-46
Barren granites
Nb/Ta = 5-16
Sn-W-(U) related granites
Zr/Hf = 18-46
Rare metals related granites Ta-Cs-Li-Nb-Be-Sn-W
Nb/Ta
Zr/Hf
Fractionated granites
Non-fractionated granites
A-type
(Na2O + K2O)/CaO
Zr+Nb+Ce+Y (ppm)
A
I-type trend
S-type trend
Th
Rb
B
Y
Rock/Chondrite
Rock/Primitive Mantle
La Ce Pr Nd Sm Eu Gd Tb Dy Ho Er Tm Yb Lu
Rb Ba Th U Nb Ta K La Ce Pr Sr Nd Zr Hf Sm Eu Ti Y Yb Lu